Quaternary Environments and Humans 3 (2025) 100049

Contents lists available at ScienceDirect

Quaternary Environments and Humans

journal homepage: www.journals.elsevier.com/quaternary-environments-and-humans

Ancient biomolecular analysis of 39 mammoth individuals from Kostenki 11-Ia elucidates Upper Palaeolithic human resource use

Alba Rey-Iglesia [a,*], Alexander J.E. Pryor [b], Deon de Jager [a], Tess Wilson [c], Mathew A. Teeter [c], Ashot Margaryan [a], Ruslan Khaskhanov [d], Louise Le Meillour [a], Gaudry Troché [a], Frido Welker [a], Paul Szpak [c], Alexandr E. Dudin [e], Eline D. Lorenzen [a,*]

[a] Globe Institute, University of Copenhagen, 1350, Denmark
[b] Department of Archaeology and History, University of Exeter, EX4 4QE, United Kingdom
[c] Department of Anthropology, Trent University, K9L 0G2, Canada
[d] Complex Research Institute of the Russian Academy of Sciences, 364051, Russia
[e] Kostenki Museum-Preserve, Voronezh 396815, Russia

ARTICLE INFO

Handling Editor: Dr Bello Silvia

Keywords:
Mammoths
Kostenki
Ancient DNA
Palaeoproteomics
Stable isotope analysis

ABSTRACT

Circular structures made from woolly mammoth bones are found across Ukraine and west Russia, yet the origin of the bones remains uncertain. We present ten new mammoth radiocarbon dates from the largest circular structure at Kostenki 11-Ia, identifying two mammoth mandibles ~200–1200 years older than the other dated materials from the site, suggesting skeletal material from long-dead individuals was scavenged and used in the site construction. Biomolecular sexing of 30 individuals showed a predominance of females, suggesting the Kostenki mammoths are primarily from herds. We identify seven mitochondrial lineages across 16 samples, and thus the mammoths are not all from the same matriline. Integrating biomolecular sexing with stable $\delta^{13}C$ and $\delta^{15}N$ isotope analysis, we find no isotopically-differentiated resource use by females and males, providing the first analysis of foraging differences between sexes in any Late Pleistocene megafauna. Our study highlights the significance of integrating ancient biomolecular approaches in archaeological inference.

1. Introduction

Kostenki 11 (also known as Anosovka 2) is an archeological site embedded in a complex of 26 Upper Palaeolithic sites situated around the villages of Kostenki and Borshchevo in south-western Russia (Voronezh Oblast; Fig. 1A) (Sinitsyn, 2015). The site is formed by several archeological layers. Five of these layers (layers Ia-V) have been well characterised (Dinnis et al., 2018); based on radiocarbon ages, they date from ~40,000 (layer V) to ~24,000 (layer Ia) calibrated years before present (cal BP) (Sinitsyn, 2015).

The Kostenki 11 site contains three circular mammoth bone complexes in layer Ia (referred to here as Kostenki 11-Ia; Fig. 1B) (Pryor et al., 2020). Circular complexes made from the bones of woolly mammoths (*Mammuthus primigenius*) are known from across the North European Plain and the East European Plain. Most are found along the Desna/Dnepr River systems in present-day Ukraine and Russia (Iakovleva, 2015, 2016), and radiocarbon dating has indicated their usage ~26,000–14,000 cal BP, with the majority of dates between 18,800 and 17,000 cal BP (Iakovleva, 2015, 2016). The complexes are usually associated with pit features potentially used for storing food or fresh bones, or discarding refuse, and indicate the past existence of open-air human settlements adapted to the steppe environment (Marquer et al., 2012), while some studies also suggest these complexes may have been used as ceremonial sites (Gavrilov, 2015; Sablin et al., 2023).

Kostenki 11 was discovered in 1951. The first mammoth-bone complex at the site was excavated during the 1960s and is now encapsulated and on display in the main building of the Kostenki Museum-Preserve (Rogachev and Popov, 1982). A second complex was discovered in close vicinity in 1970 and was only partially excavated (Rogachev and Popov, 1982). These two mammoth complexes each encompass a large central (9–10 m diameter) circular structure made of mammoth bones, surrounded by storage pits (Fig. 1B).

The third mammoth-bone complex is the focus of the present study

* Corresponding authors.
E-mail addresses: alba@palaeome.org (A. Rey-Iglesia), elinelorenzen@sund.ku.dk (E.D. Lorenzen).

https://doi.org/10.1016/j.qeh.2024.100049
Received 19 August 2024; Received in revised form 4 December 2024; Accepted 9 December 2024
Available online 11 December 2024

and was discovered adjacent to the Kostenki Museum-Preserve building during a survey in 2013–2014 (Dudin and Fedyunin, 2019). The structure is placed 20 m from the first bone complex (Fig. 1B). It is a large circular structure with at least three peripheral pits, and is a more sophisticated entity than the other two complexes at Kostenki 11-Ia. It is larger both in size (with a central cluster of 12 ×11 m) and in the sheer number (n = 2982) of mammoth bones found, with a minimum of 64 individuals identified based on the number of mammoth crania (Fedyunin, 2016; Dudin, 2017) (Fig. 1C, Tables S1, S2). Previous radiocarbon dating of charcoal and faunal remains (including burnt mammoth bone) from the third complex indicate that it is one of the oldest such structures associated with modern humans yet discovered on the eastern European Plain (Pryor et al., 2020).

The mammoth bones of the third complex have been investigated and described based on morphology, and extensive work has been conducted on the identification of various skeletal elements, their positioning and preservation, including the presence of animal gnawing and chewing marks and anthropogenic cut marks and notches (e.g., Dudin and Fedyunin, 2019). However, additional methods are required to answer several outstanding questions, including a more reliable time frame of when and for how long Palaeolithic humans were associated with the site, and how Palaeolithic humans procured the mammoth resources used to form this structure.

Ancient biomolecules provide the toolbox necessary to further investigate the site (Swift et al., 2019). Radiocarbon dating can be used to infer when the site was in use, ancient DNA can be used for genetic sex determination of the mammoth individuals in the complex and to elucidate the phylogeographic context of the mammoths. Where ancient DNA is insufficiently preserved, ancient protein analysis may provide an alternative approach to determining genetic sex through the analysis of dental enamel. Stable isotopes contribute information on the dietary niche of mammoth individuals, and may elucidate differences in foraging ecology between females and males when used in conjunction with genetic sexing.

Due to its rich fossil record and emblematic status as a flagship species of the extinct Late Pleistocene megafauna, woolly mammoths remain one of the most well-studied species of the Eurasian mammoth steppe (e.g., Arppe, 2019; Chang, 2017; Pečnerová, 2017a, 2017b.

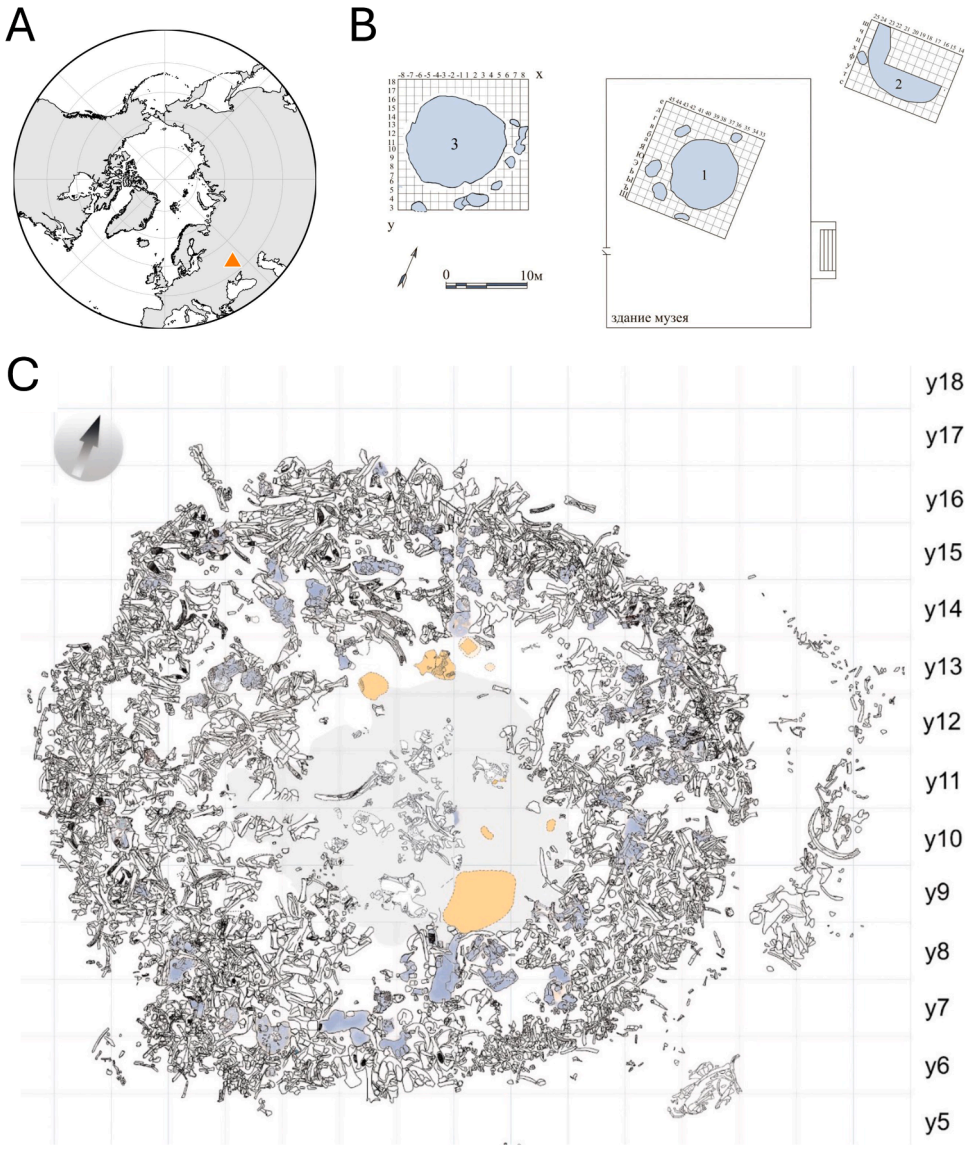

Fig. 1. The Kostenki 11 site. (A) North polar projection map indicating the location of the site. (B) Relative locations of three mammoth-bone complexes in Kostenki 11-Ia (image credit: I.V. Fedyunin of LLC 'Terra'). The first structure (middle) is preserved today in the Kostenki Museum-Preserve, and the second structure has only been partly investigated. (C) Site plan of the third mammoth-bone structure as it appeared at the end of the 2015 excavation season; blue indicates crania and yellow indicates fires (hearth and surface fires). The site measures 12 m across and includes 2982 mammoth bones, and 64 crania.

During the last glacial period ~115,000–12,000 yr ago, mammoths were widely distributed across Eurasia and extended into the northern half of North America (e.g. Puzachenko et al., 2017). Radiocarbon dated mammoth remains have been widely investigated using ancient biomolecular approaches, including ancient DNA and stable isotopes, providing insights into their movement patterns, population histories, and palaeoecology. Indeed, the oldest nuclear genome ever sequenced is from a 1.6 million year old Siberian mammoth (van der Valk et al., 2021). Hence for this species, a rich panel of reference data exists with which to contextualise ancient biomolecular information from new specimens.

Woolly mammoths are believed to have had a matriarchal social structure, where adult females form groups with their offspring, and adult males leave the herd or form small, temporary bachelor groups, as this trait is shared by all extant proboscideans (Wittemyer et al., 2007). This hypothesis is supported by morphological analysis of mammoth bone assemblages, such as the Sevsk woolly mammoth family group (Bryansk Region, Russia), which comprised a mix of females and males of different ages (Maschenko et al., 2006). Male-dominated sites of the Columbian mammoth (*Mammuthus columbi*), such as at the Hot Springs locality (South Dakota, USA), are believed to represent individuals outside a family group (Lister and Agenbroad, 1994). However, morphological sex determination may not be reliable or indeed even possible for most fossil specimens. There have been no previous attempts to genetically sex the skeletal remains present in the mammoth complexes from the central European Plain, including Kostenki 11-Ia. This information may provide novel insights into the origin of the skeletal remains and the hunting behaviour of prehistoric humans.

The retrieval of ancient DNA from mammoth remains has provided evidence of the biogeography of mammoths across time and space, detailing how and when mammoth genetic lineages moved across the landscape (termed phylogeography) (e.g., Chang, 2017; Debruyne, 2008; Enk, 2016; Palkopoulou, 2013). Synthesis of the available mitochondrial genome data from mammoths shows the species can be divided into three main, genetically distinct groups (Chang et al., 2017). Although the three groups are all widely distributed across the landscape, the geographic distribution of specific subclades within each genetic group can in some cases provide information as to the geographic origin of an individual (e.g., Chang, 2017; Debruyne, 2008).

Bone and dentine collagen carbon ($\delta^{13}C$) and nitrogen ($\delta^{15}N$) stable isotopes provide data on the foraging ecology of individuals. In herbivores, the data provide information on the relative importance of types of plant species in the diet. The composition of plants in the diet (Smith and Epstein, 1971) is indirectly affected by climatic and environmental factors (Murphy and Bowman, 2006; Hartman, 2011; Bonafini et al., 2013) and can therefore be further used to make inferences about the palaeoecology of the environment inhabited by individuals/species.

In this study, we used a combined biomolecular approach of radiocarbon dating, ancient DNA, palaeoproteomics, and stable $\delta^{13}C$ and $\delta^{15}N$ isotope analysis, to investigate 39 woolly mammoth individuals collected from the third residential complex of Kostenki 11-Ia. Our findings represent: (i) ten new ^{14}C dates, which are discussed in the context of other available direct dates from Kostenki 11-Ia, to infer the time frame of human activity at the site; (ii) combined genetic and proteomic sexing of 30 specimens, which provide indirect insights into resource use of Palaeolithic humans; (iii) mitochondrial genomes of 16 individuals, which we analysed with 147 publicly available mitochondrial genomes, to investigate the matrilineal composition of the site and the phylogeographic context of the mitochondrial sequences; and (iv) $\delta^{13}C$ and $\delta^{15}N$ values from 38 individuals, which we analysed with 378 available records from mammoths sampled across time and space, to detect resource partitioning between the sexes and characterise the paleoecology of the Kostenki mammoths.

2. Material and methods

2.1. Experimental design

We performed biomolecular analysis of 39 woolly mammoth specimens sampled from the third mammoth bone complex at Kostenki 11-Ia. We radiocarbon dated nine specimens (one specimen was dated twice, totalling ten dates), and used the ages to interpret the time frame of human activity at the site. Combining ancient DNA and palaeoproteomic methods, we sexed the mammoth individuals, and used the data to identify the ratio of females and males at the site. By integrating biomolecular sexing with stable $\delta^{13}C$ and $\delta^{15}N$ isotope analysis, we investigated differences in isotopically-differentiated resource use by females and males. Mitochondrial genomes and paleoecological ($\delta^{13}C$ and $\delta^{15}N$) data from the Kostenki 11-Ia individuals were contextualised within the frameworks of available data from other late Quaternary woolly mammoths.

2.2. Mammoth specimens

A minimum of 51 mandibles and 64 crania from mammoths had been excavated at the third mammoth bone complex at Kostenki 11-Ia by the end of 2015 (Voronezh, Russia; Fig. 1C) (Dudin, 2017). E.D.L. and A.M. visited the site in August 2015 to collect mammoth faunal material for ancient biomolecular work (Fig. 2). At that time, 40 mandibles had been unearthed and could be identified in the complex. To ensure that each sample represented a unique individual, protruding molars of the left mandible were sampled for 37 individuals. For two individuals, where the mandible was deposited upside down, direct access to the tooth was not possible and instead bone from the left mandible was sampled (Table S3).

As the excavation was still ongoing when we visited the site, we are unable to reliably match the 39 sampled individuals *post hoc* with the distribution of mammoth bones in the final site map (Fig. 1C).

The sampled mandibles varied in size and most likely represent both adults and juveniles (Fig. 2C). However, no data are available on the relative size of the individuals sampled. In 2016, 44 (out of 45 unearthed open mandibles) were measured, revealing that some were significantly smaller (Dudin, 2017). However, a more comprehensive analysis is still required to determine whether these smaller specimens are juvenile mammoths. In addition, in-depth analysis on the anthropogenic modifications on the mammoth bones is ongoing.

For ease of reference, we have excluded the prefix of 'CGG_1_0' from the specimen IDs – e.g. specimen CGG_1_018221 is designated 18221 – and only use the last five digits in the text, figures, and tables.

2.3. Radiocarbon dating

Nine specimens were selected for radiocarbon dating at the Keck Carbon Cycle AMS Facility (Earth System Science Department, UC Irvine) (Table S3). Not all samples were radiocarbon dated due to limited resources and the cost of the procedure. Subsampling of the specimens was conducted at the ancient DNA clean lab facilities at Globe Institute (University of Copenhagen), and collagen was extracted at Trent University (Beaumont et al., 2010). 100–200 mg of bone/dentine chunks were demineralized in 0.5 M HCl until completely demineralized. Samples were then rinsed to neutrality with ultrapure water. Any samples exhibiting a dark discoloration were treated with 0.1 M NaOH for successive 20 min treatments until no colour change was observed in the solution. Samples were rinsed to neutrality with ultrapure water. All demineralized samples were then placed in 4 mL of 0.01 M HCl and the collagen was solubilized at 65°C for 36 h. The resulting solution containing the collagen was then filtered using 30 kDa centrifugal filters (Centriprep, Millipore) that were cleaned according to Beaumont et al., 2010. The > 30 kDa portion was then transferred to a glass vial, frozen and lyophilized.

Fig. 2. The third mammoth bone complex at Kostenki 11-Ia. (A) An overview of the third structure. (B) Specimen 18234 (field ID 17); we were unable to retrieve DNA or amelogenin for biomolecular sexing of this individual. (C) Close-up of the mammoth bones forming the structure, showing six mandibles of various size. (D) Specimen 18232 (field ID 15), which we genetically sexed as a male and identified as Hap74, a mitochondrial haplotype unique to our dataset. Photos: (A) A. Dudin; (C-D) E.D. Lorenzen.

We calibrated the radiocarbon dates in OxCal v.4.4 (Bronk Ramsey, 2021) using the IntCal20 (Reimer et al., 2020) calibration curve. Two of the dates (UCIAMS-251304 from specimen 18222; UCIAMS-251305 from specimen 18241) were younger than our expectations based on the archeological chronology. Therefore, we re-sampled the two specimens and carried out new collagen extractions for an additional round of dating. However, one specimen (18222) did not yield enough collagen to provide a second date, resulting in a final dataset of ten new radiocarbon dates (Table S3). With each batch of samples for which collagen was prepared for radiocarbon dating, one or more aliquots of a sample with an infinite radiocarbon age (Hollis Mine mammoth, FmC = 0.0031 ± 0.0002) (Martinez De La Torre et al., 2019) and a secondary standard of known age (Umingmak whale, 7325 ± 40 BP) (Crann et al., 2017) were prepared in the same manner as the samples, and radiocarbon dated. These standards returned radiocarbon ages very similar to their long-term measured values: FmC = 0.0031 ± 0.0009 for the Hollis Mine Mammoth and 7340 ± 20 BP for the Umingmak whale.

We combined the total of ten dates (including the two dates generated for specimen 18241) with 14 available radiocarbon dates from Kostenki 11-Ia from the first and third complexes at the site (Table S4), to create an overview of the chronology of this site, using in OxCal v.4.4 (Bronk Ramsey, 2021) and IntCal20 (Reimer et al., 2020). Available dates comprise four charcoal dates and ten mammoth bone dates (Pryor et al., 2020; Rogachev and Popov, 1982; Popov et al., 2004; Praslov and Soulerjytsky, 1997; Sinitsyn et al., 1997). Further analysis was conducted on a reduced dataset – excluding erroneous dates and also dates measured with low precision – using OxCal v.4.4 (Bronk Ramsey, 2021), with the IntCal20 calibration curve (Reimer et al., 2020). This reduced dataset comprised eight new radiocarbon dates reported here, and three previously measured charcoal dates. Further details are provided in the Supplementary Text.

2.4. Ancient DNA extraction and sequencing

We drilled 50–70 mg of bone or dentine powder from each mammoth specimen. DNA extractions were carried out following two different protocols: a silica-powder based method and a silica column method (Table S5). The silica-powder method is based on the protocol published in Rohland and Hofreiter (2007) with some modifications following Allentoft et al. (2015). We included a pre-digestion and a modified binding buffer as described in Allentoft et al. (2015). The modified binding buffer was prepared in bulk by mixing 500 mL Qiagen buffer PB with 9 mL sodium acetate (5 M) and 1.25 mL sodium chloride (5 M). After mixing the pH was checked and corrected until reaching a value between 4 and 5.

The second DNA extraction protocol used a modified version of a silica-column based protocol (Dabney et al., 2013). Dentine/bone powder was incubated overnight at 37°C with constant rotation in 1 mL of extraction buffer. After the overnight incubation, the supernatant was added to a 30 kDa Amicon® Ultra-4. The sample was centrifuged at 4000 rpm, until the supernatant was concentrated down to 70 μL. The concentrate was combined with 10x modified Qiagen PB buffer as described in Allentoft et al. (2015) and purified using Monarch columns (NEB). After DNA binding to the Monarch columns, we performed two washes with Qiagen PE. DNA elution was performed in two steps; for every step, we added 25 μL of Qiagen EB buffer to the Monarch column, incubated for 5 min at room temperature, and centrifuged at 13, 000 rpm (max speed) for 1 min.

Some of the DNA extracts were treated with Thermolabile USER II enzyme (NEB) prior to library build (Table S5). For each sample, the USER reaction was performed in 16 μL total volume, with 2.4 μL of the Thermolabile USER II enzyme and 13.6 μL of each extract, and incubation time of 3 h at 37°C. USER treated DNA extracts were purified using Monarch columns (NEB).

We used two different library build protocols: a double stranded DNA (dsDNA) (Meyer and Kircher, 2010) and a single stranded DNA (ssDNA) (Kapp et al., 2021) method (Table S5). For the dsDNA library build, we used the protocol described in Meyer and Kircher, 2010 with the following modifications: our reaction volume was 25 μL, the initial DNA fragmentation was not performed, and MinElute kit (Qiagen) was used for the purification steps. The ssDNA libraries were built following the procedure described in Kapp et al., 2021. Only the USER treated extracts were used for the ssDNA protocol.

All the libraries were double-indexed using KAPA HiFi HotStart Uracil+ReadyMix (Roche). The resulting indexed libraries were quantified on a Qubit™ dsDNA HS (Invitrogen) and quality checked in the Agilent BioAnalyzer or Fragment Analyzer. Indexed libraries were shotgun sequenced on an Illumina HiSeq 2500 SE80 base pairs (bp) or NovaSeq 6000 PE150 bp.

2.5. Bioinformatic data processing

Adapter and quality trimming with AdapterRemoval v2.2.0 (Schubert et al., 2016), mapping (read alignment, PCR duplicate removal, and indel realignment), and mapDamage v2.0.6 analyses (Jónsson et al., 2013) of the shotgun data were performed using the PALEOMIX pipeline v1.3.6 (Schubert et al., 2014). Mapping was performed using the BWA-aln v0.7.17 (Li and Durbin, 2009) with seed length disabled to improve mapping efficiency (Schubert et al., 2012). Reads shorter than 30 bp were discarded during adaptor trimming and reads showing mapping qualities less than 30 were also excluded. For PE150 data only collapsed reads were used, as non-collapsed paired-end reads are more likely to be contaminants. For mapping, we used the nuclear genome assembly of the African savannah elephant (*Loxodonta africana*; LoxAfr4, available at ftp://ftp.broadinstitute.org/pub/assemblies/mammals/elephant/loxAfr4/) and a woolly mammoth mitochondrial genome (mitogenome) reference (GenBank: DQ188829.2).

We generated mitogenome consensus sequences for the three samples that had > 1000 reads mapping to the mitogenome reference (Tables S3, S5). We generated the consensus sequences using Geneious R11 (Kearse et al., 2012) using the strict criteria requiring more than 50 % of reads for each base to match for bases with a coverage > 3x. Bases with coverage < 3x or ambiguous bases were called as undetermined (N).

2.6. Mitochondrial genome capture

To increase the number of mitochondrial sequences, we performed mitochondrial enrichment by target capture on the 20 ssDNA libraries using a myBaits (MYcroarray/Arbor Biosciences) custom-design mitochondrial genome array, which included baits designed based on a mammoth mitogenome reference (DQ188829.2).

The myBaits v5.01 High Sensitivity protocol was used with hybridization at 55°C at all relevant steps, with the only deviation from the protocol being that only one round of enrichment was done, with a ratio of 1:4 baits:water in the hybridization mix.

Post-capture amplification was performed using NEBNext Q5U Master Mix (New England Biolabs) as follows: 98℃ for 2 min, 18 cycles of 98℃ for 20 s, 60℃ for 30 s, and 72℃ for 45 s, with a final extension step of 72℃ for 5 min. The captured libraries were pooled equimolar and sequenced on an Illumina NovaSeq X Plus PE150 bp. The data processing of these reads was performed with PALEOMIX as above, except that reads were only mapped to the woolly mammoth reference mitogenome.

Consensus sequences were generated in Geneious as above for the 14 samples with > 900 reads mapping to the reference (Table S5).

2.7. Genetic sex determination

We performed genetic sex determination of the 23 mammoth specimens that had > 5000 reads (Bro-Jørgensen et al., 2021) from the shotgun sequencing mapping to the nuclear genome assembly of the African savannah elephant. Sex determination was performed as described in Pečnerová et al., 2017a. We estimated the ratio of the number of reads mapping to sex chromosome X *versus* an autosome. We used chromosome X (ChrX) and chromosome 8 (Chr8), which are of comparable size. As female mammals have two copies of chromosome X, and males carry only one copy, we expected ChrX:Chr8 ratios of ~0.5 for males and ~1 for females. The number of reads mapping to ChrX and Chr8 was obtained using samtools idxstats (Li et al., 2009). To correct for chromosome size differences, the number of mapped reads was normalised by the length of the chromosomes (Table S5). Samples were determined as males if ChrX:Chr8 < =0.7, females ChrX:Chr8 > =0.8, and undetermined if ChrX:Chr8 0.7–0.8.

2.8. Proteomic sex determination

Dental powders of 21 mammoths were provided for palaeoproteomic dental enamel sex assignment (Table S7). Of these specimens, three were male and three were female based on our ancient DNA sex assignment (see above), while the remaining 15 specimens could not be sexed based on ancient DNA analysis (Table S3).

Dental enamel proteomes are dominated by peptides resulting from the *in vivo* hydrolysis of amelogenin. Amelogenin isoforms located on the X-chromosome and Y-chromosome have different amino acid sequences for some mammalian clades, allowing the proteomic sex assignment of, for example, human individuals through the observation of peptides uniquely matching to amelogenin-Y (AMELY) as male individuals. In contrast, the absence of AMELY-specific peptides combined with an abundance of AMELX-specific peptides is often taken to suggest a female sex assignment (Stewart et al., 2017; Parker et al., 2019; Cintas-Peña et al., 2023). Since dental enamel proteomes preserve over longer periods of time than ancient DNA, the proteomic determination of genetic sex provides an alternative molecular approach to study sex-based differences in hunter-gather ecology and Pleistocene faunal ecologies.

These enamel powders were immersed in 1 mL of 5 % hydrochloric acid (HCl) and placed at 4℃ overnight. The following day, samples were centrifuged for 10 min at 3000 *g* and supernatants collected into new tubes (labelled S1). Another mL of HCl was added for another 12 hours. After the last 12 hours, the samples were not completely demineralised and were placed on a carousel at room temperature to ensure complete demineralisation. After the additional 12 hours, the samples were demineralised, and were centrifuged using the same parameters as before. The supernatants were collected into new tubes (labelled S2) before being placed at −18℃ until further steps. Each extract was then loaded on an individual Evotip (Evosep, Odense, Denmark) as follows: 500 μL of S1 and 500 μL of S2 were first combined in S3 tubes; S3 solutions were acidified with the addition of 1 μL of TFA (100 %) and finally, 2 × 200 μL of S3 solutions were loaded on the corresponding Evotip following the standard recommended protocol (Bache et al., 2018). An extraction blank was performed alongside the samples, and analysed using liquid chromatography coupled to tandem mass spectrometry (LC-MS/MS). This blank remained empty of any protein matches to dental enamel proteins, including an absence of albumin and collagen type I (COL1) peptides.

Extracts were first separated by liquid chromatography on an Evosep One (Evosep, Odense, Denmark) using the 60SPD method with a gradient of 21 min for a total cycle of 24 min. Separation was conducted using a polymicro flexible fused silica capillary tubing (150 μm inner diameter, 16 cm long) home-pulled and was packed with C18 bonded silica particles (1.9 μm diameter, ReproSil-Pur, C18-AQ, Dr. Maisch, Germany) with mobile phases consisting of A: 5 % acetonitrile and

0.1 % formic acid in H_2O and B: 0.1 % formic acid in H_2O at a flow-rate of 2 μL/min. The mass spectrometer, an Exploris 480 (Thermo Fisher Scientific) was set on data dependent acquisition mode with a first MS1 scan at resolution of 60,000 on the *m/z* range 350–1400. The twelve most intense monoisotopic precursors were selected, and were then dynamically excluded after one appearance with their isotopes (± 20 ppm) for 20 seconds. The selected peptides were acquired on MS2 with the Orbitrap with a resolving power of 15,000, HCD set at 30 %, quadrupole isolation width of 1.3 *m/z* and a first *m/z* of 120.

In the absence of available amelogenin sequences for mammoths, we built a protein reference database containing entries for 12 proteins (COL1A1, COL1A2, COL17A1, AMELX, AMELY, TUFT1, AMBN, AMLT, ALB, ENAM, ODAM, and MMP20) for *Elephas maximus* and *Loxodonta africana* derived from Genbank and UniProt. The database included 16 amelogenin isoforms across both taxa, including a single, nearly complete AMELY sequence. Proteomic data analysis was conducted in Maxquant v2.1.3.0 using unspecific digestion settings, allowing for a maximum of 5 variable PTMs (deamidation (NQ), phosphorylation (STY), and oxidation (MP)). Peptides were allowed to be between 7 and 30 amino acids, with a minimum score of 40, and filtered up to 1 % FDR at peptide and protein level. Other settings were left as default. Based on the results of the genetically sexed female and male mammoth individuals, minimum peptide thresholds were determined to allow the confident identification of female individuals (based on reaching a minimum number of 15 AMELX-specific peptides) and male individuals (based on reaching a minimum number of 2 unique AMELY-specific peptides). These thresholds may differ depending on mass spectrometry data acquisition settings, extraction method, or data analysis approach, and are therefore not general recommendations for future studies.

2.9. Mitochondrial phylogeography

To determine which known genetic group/s (clade/s) the Kostenki mitogenomes belong to, we compiled 166 mammoth mitogenomes available in GenBank (data downloaded on 07–05–2021). Those shorter than 16,450 bp or that had > 20 % N bases were excluded from downstream analyses, leaving a reference panel of 147 mitogenomes (Table S6). Of the 16 Kostenki mitogenomes generated, three had > 20 % N bases (18225, 18236, and 18255) and were initially excluded from the phylogeographic analysis. Thus, a total of 160 mitogenomes were aligned using the MAFFT (Katoh and Standley, 2013) plugin v1.5.0 in Geneious. Due to potential misalignments and missing data, we removed the d-loop from the final alignment.

To estimate the number of haplotypes (unique sequences) present in the data we used Mesquite v3.81 (Maddison and Maddison, 2023) to convert all uncertainties (e.g. ambiguous bases) in the alignment to missing data, and used this alignment in DnaSP v6.12 (Rozas et al., 2017) to assign sequences to haplotypes by generating a haplotype data file. Sites with gaps or missing data were not considered.

To investigate the evolutionary relationships of the haplotypes, we used the same alignment from Mesquite in PopART v1.7 (Leigh and Bryant, 2015) to generate a median-joining haplotype network. For the three Kostenki mitogenomes that had > 20 % N bases, we performed the haplotype assignment individually because the increased amount of missing data that the N bases introduced into the alignment would otherwise have reduced the number of haplotypes and the overall power of the analysis. We nonetheless wanted to determine their relationship to the reference panel and the other Kostenki mitogenomes. Thus, each of the three (18225, 18236, and 18255) was aligned in turn with the other 160 mitogenomes and the haplotype analysis performed as before. Furthermore, for those Kostenki samples that shared a haplotype, we compared their control region (d-loop) sequences to further refine the haplotype sharing results. Since the control region is more variable and has a higher mutation rate, it would confirm that the mitogenomes were indeed identical if samples shared the same d-loop haplotype as well. The control region was extracted and aligned via MAFFT in Geneious and the sequences were compared as in the haplotype analysis above.

We also estimated a maximum likelihood (ML) phylogeny of the 90 haplotypes in IQ-TREE v2.2.0 (Minh et al., 2020), using the Asian elephant (*Elephas maximus*, GenBank: EF588275.2) as an outgroup. The mitogenome with the least missing data for each haplotype was selected and the sequences were again aligned with MAFFT in Geneious, the d-loop was removed, and uncertainties changed to missing data in Mesquite. IQ-TREE was run with automatic model testing and selection (-m MFP) (Kalyaanamoorthy et al., 2017), 1000 ultrafast bootstrap replicates (-B 1000 -alrt 1000) (Hoang et al., 2018), and two independent runs (–runs 2). The consensus tree was visualised using Figtree v1.4.4 (Rambaut, 2009) and further edited for visual clarity in Inkscape v1.3.2 (www.inkscape.org).

2.10. Molecular dating of mitogenomes

The ages of the nine Kostenki mitogenomes without radiocarbon dates and new to our study were estimated with BEAST v1.10.4 (Suchard et al., 2018). We also estimated a molecular date for the mitogenome from (Chang et al., 2017). A detailed description of the methodology is provided in the Supplementary Text.

In short, we used a subset of the 160 mitogenomes and only used mitogenomes with curated radiocarbon dates from Dehasque et al., 2021, and the four Kostenki mitogenomes with reliable radiocarbon dates from this study.

This resulted in a total of 101 mammoth sequences that were aligned (as before) with 15 outgroup sequences as used by van der Valk et al., 2021 (Table S6). Sequences with median radiocarbon dates between 40 ka and 50 ka were subsequently removed from the alignment, as this is towards the limit of radiocarbon dating and the dates may be less reliable. This resulted in 13 sequences being removed, which included all radiocarbon dated reference sequences from clades 2/A and 3/B2.

The molecular dating was conducted following the procedure and settings in van der Valk et al., 2021. The age of each sequence was estimated individually in turn, with two independent MCMC runs each with 100 million generations and sampling every 10,000 generations. Convergence was evaluated in Tracer v1.7.2 (Rambaut et al., 2018) and the age of each molecularly dated sequence obtained from the combined log files (LogCombiner v2.6.7, 20 % burnin) as viewed in Tracer.

2.11. Stable isotope analysis

A tooth or bone fragment of 100–300 mg was cut from each sample using an Ultimate XL-D micromotor. For mammal juveniles, tooth and bone can yield higher $\delta^{15}N$ values compared to adults due to suckling as lactate is ^{15}N-enriched, which results in an enrichment in $\delta^{15}N$ in the developing tissues (Balasse and Tresset, 2002; Balasse and Tresset, 2002). Some of the mandibles sampled at Kostenki 11-Ia were of smaller size, thus we assume they belonged to juveniles. In addition, for the tooth, we did not target a specific layer, but rather cut a random sample consisting of several layers, therefore reducing the influence of the suckling effect for those mandibles putatively belonging to juveniles. Each fragment was then crushed into smaller pieces using a Plattner mortar and a pestle. The crushed fragments were immersed in 9 mL of 0.5 M hydrochloric (HCl) acid at room temperature for demineralization. Throughout the demineralization treatment, the samples were agitated on an orbital shaker. Samples remained in acid between 17 and 30 h and were removed from the demineralization solution when the fragment was soft and/or floating in solution. Immediately upon removal from the demineralization solution, each sample was rinsed four times in 10 mL of Type I water (resistivity >18.2 MΩ cm).

Following demineralization, the samples were solubilized in 3.5 mL of 0.01 M HCl at 75°C for 36 h. The samples were centrifuged to precipitate the insoluble material, and the collagen suspended in solution was transferred into a glass vial and frozen for 24 h. Once frozen, the

collagen samples were lyophilized for 48 h. Dried collagen weighing between 0.5 and 0.6 mg was transferred into tin capsules for stable isotope and elemental analysis. These analyses were performed at the Trent University Water Quality Centre using a Nu Horizon continuous flow isotope ratio mass spectrometer paired with a EuroVector EA 300 elemental analyzer. The stable isotope results were calibrated using Vienna Pee Dee Belemnite (VPDB) for $\delta^{13}C$ and AIR (ambient inhalable reservoir) for $\delta^{15}N$. International reference standards USGS40 and USGS66 were used to perform these calibrations. In-house laboratory standards SRM-1 (caribou bone collagen), SRM-2 (walrus bone collagen), and SRM-14 (polar bear bone collagen) were used to monitor analytical accuracy and precision of the analyses.

To investigate potential differences between the sexes in their isotopic niche, we combined $\delta^{13}C$ and $\delta^{15}N$ for the two sexes in RStudio using ggplot (Wickham, 2011) to estimate the 95 % confidence ellipses for each dataset, and the average and standard deviation. Due to the limited number of records for each of the sexes, statistical tests were not further performed.

To contextualise the data within a spatiotemporal framework, we compiled available $\delta^{13}C$ and $\delta^{15}N$ records for woolly mammoths from bone and dentine collagen. We used Web of Science to perform a literature search with the terms "woolly mammoth" and "stable isotope", and "*Mammuthus primigenius*" and "stable isotope" (data search 25/08/2021). We recovered isotope records for 378 woolly mammoths (Table S8). The data were divided into four geographical regions: Eastern Beringia (E Beringia; Yukon and Alaska; n = 129), Northern Siberia (N Siberia; Chukotka, Yakutia, and Taymyr; n = 183), Russian Plain (n = 16), and Western and Central Europe (W/C Europe; n = 50). As specific LAT and LON coordinates were not available for the majority of the sites, we have not provided maps of the groups, but indicate the regional affiliation of each data point in Table S8. The 95 % confidence ellipses, average, and standard deviation for each region were estimated as indicated above.

Kostenki 11-Ia has been dated to the Last Glacial Maximum (LGM; 28,660–20,520 cal BP) (Kuitems et al., 2019). Therefore, to reduce biases due to temporal variation in isotopic composition caused by climatic and vegetation changes, we also performed a comparison limited to woolly mammoth LGM records (n = 44 published records). Number of records used for this analysis was: E Beringia n = 6, N Siberia n = 23, Russian Plain n = 5, and W/C Europe n = 10, in addition to the new records generated from Kostenki.

3. Results

3.1. Radiocarbon dating

We radiocarbon dated nine woolly mammoth individuals from the third mammoth bone complex at Kostenki 11-Ia; one individual was dated twice, yielding a total of ten dates (Table S3). None of the woolly mammoth specimens sampled showed any evidence of burning. Thus, we assume the radiocarbon ages of these specimens have not been altered by fire.

Radiocarbon dating initially produced two dates younger than the rest of the dates new to this study, and also younger than most of the existing dates for the third mammoth complex (Fig. S1, Tables S3, S4): UCIAMS-251304 (18222; genetically sexed as female) and UCIAMS-251305 (18241; genetically sexed as female) with radiocarbon ages 18,080 ± 60 BP and 18,870 ± 70 BP, respectively. Both specimens were therefore re-dated using freshly extracted collagen taken from different parts of the molar.

Specimen 18222 failed the re-dating due to an insufficient amount of collagen. Specimen 18241 produced a second radiocarbon date of 20,400 ± 140 BP (UCIAMS-266002), similar to the other radiocarbon dates new to this study, with a median age more than 1500 radiocarbon years older than the first dating attempt, confirming that our two younger dates are almost certainly a result of incomplete removal of contamination during pre-treatment, exacerbated by a relatively low weight of endogenous collagen for these specimens. Difficulties with removing exogenous younger carbon contamination from collagen samples used for dating is a well-known problem with Palaeolithic material, including from other Kostenki sites (e.g., Dinnis, 2019; Herrando-Pérez, 2021; Reynolds et al., 2017).

The eight remaining and reliable dates were added to three previously reported dates measured on charcoal recovered from inside the third mammoth bone complex (Supplementary Text), together giving 11 dates with unmodeled median calendar ages spanning 25,460–24,390 cal BP (Fig. 3A).

We analysed these dates using Oxcal's 'Combine' function, which combines probabilities from multiple dates each giving independent information on the age of a specific sample or context (Bronk Ramsey, 2021). The method may, where appropriate, include dates measured on different materials using different methods (e.g. ^{14}C, TL, OSL). Importantly, the method assumes that the activity being dated occurred within a 'short' time frame relative to the uncertainties associated with the dates being modelled; in this case approximately 500–1000 years for the calibrated dates. It is therefore appropriate to use the 'Combine' function to model dates from the third mammoth bone complex at Kostenki 11-Ia, assuming that any phase, or phases, of activity lasted for a brief period relative to the dating uncertainty, in this case not exceeding a few hundred years at most (Bronk Ramsey, 2021). This assumption is well supported by the archaeological evidence at Kostenki 11-Ia, which indicates that human activity at the site actually occurred over a much briefer period or periods, lasting a few years or decades at most (Pryor et al., 2020; Dudin and Fedyunin, 2019). We note here the difference between Oxcal's 'Combine' and 'R_Combine' functions, the latter of which is designed to combine radiocarbon dates measured on the same artefact, and which would be inappropriate for analysing the Kostenki 11–1a dates.

When the 11 radiocarbon dates for Kostenki 11-Ia are modelled as a single group using Oxcal's 'Combine' function the analysis fails with an overall A'Comb of just 2.6 %. In particular the two oldest radiocarbon dates are substantially older than the nine other dates and show very poor agreement with the rest of the dataset. Splitting off the two oldest dates and re-running the analysis combining just the nine youngest dates moderately improves the model result (A'Comb of 41 %). However, the results are improved further by dividing the dates into a total of three groups, apparently reflecting multiple age populations within the radiocarbon dataset (Fig. 3A). The earliest group comprises two dates measured on mammoth teeth, which are notably older than all other measured dates from the site. The molars – both genetically sexed as female – were located in the outer ring of the structure (Fig. S2).

The next group includes five dates measured on both mammoth teeth and charcoal (termed 'Phase 1', Fig. 3A) which have a modelled date range of 25,040–24,670 cal BP while the youngest group, comprising one date on charcoal and three on mammoth teeth (termed 'Phase 2', Fig. 3A) which have a modelled date range of 24,580–24,230 cal BP. There is excellent statistical agreement between the modelled Phase 1 and Phase 2 dates, respectively, with A'Combs above 140 %.

The calibrated ages for our Phase 1 are remarkably similar to those indicated for Group 1 dates by Pryor et al (Pryor et al., 2020)., supported by three dates new to this study. In contrast, calibrated ages for Phase 2 are several hundred years older than Pryor et al., 2020 Group 2 dates, as a direct consequence of focusing on the relatively high-precision CURL and UCIAMS radiocarbon dates, and setting aside the less-precise and likely contaminated NSKA dates (Supplementary Text).

3.2. Genetic analysis

We estimated the endogenous DNA content of our 39 specimens by mapping the DNA sequencing reads to the nuclear genome assembly of the African savannah elephant (*Loxodonta africana*; LoxAfr4). Overall, most of the specimens had very poor DNA preservation. Endogenous

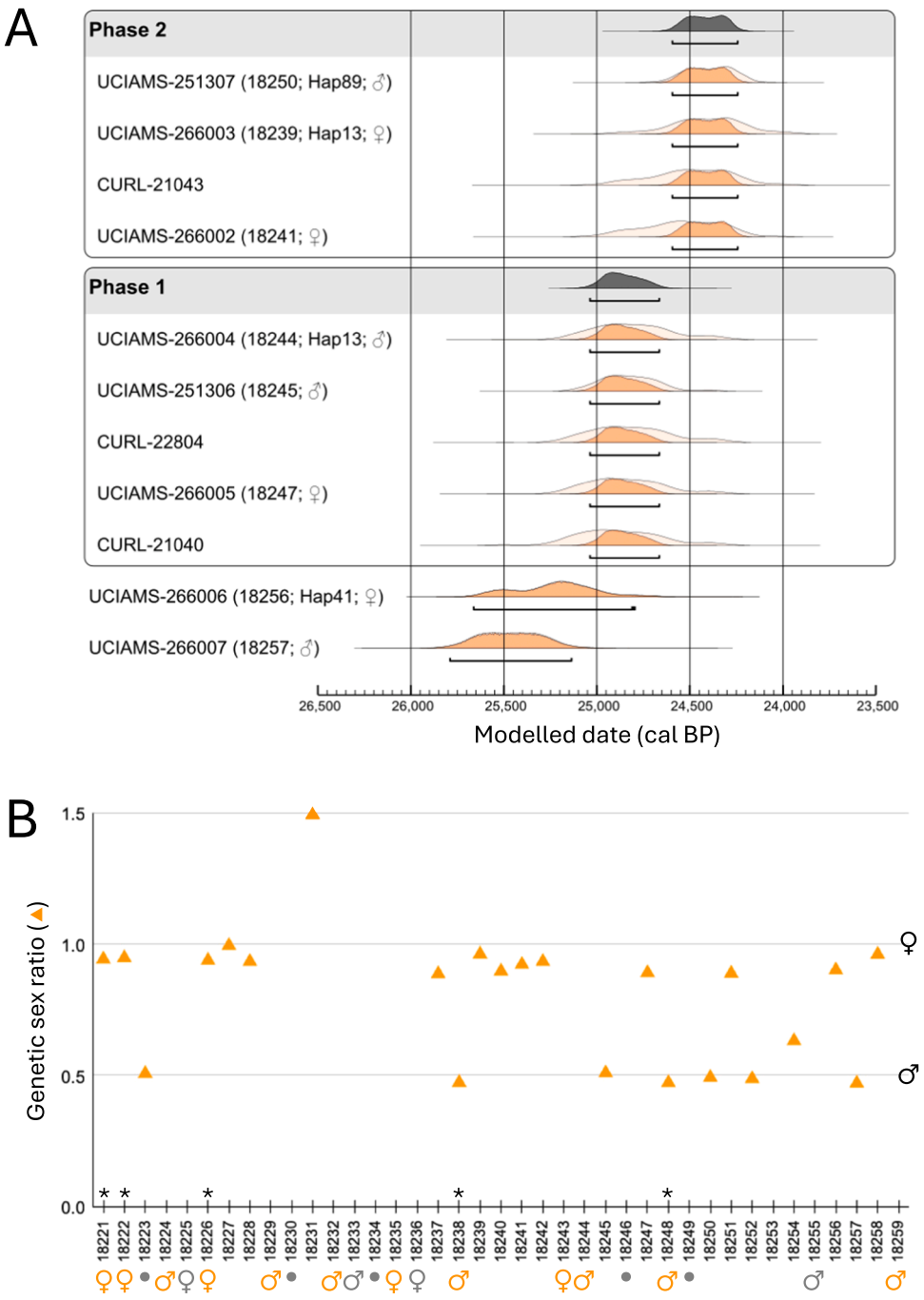

Fig. 3. Phases of human activity and biomolecular sex of the Kostenki 11 mammoths. (A) New (UCIAMS, all unburnt mammoth bones) and published (CURL, all charcoal) radiocarbon dates from the third mammoth bone complex. We used the 'Combine' function in OxCal v. 4.4 (Bronk Ramsey, 2021) to determine two discrete phases of human activity at the site: Combine Phase 1 (25,040–24,670 cal BP) and Combine Phase 2 (24,580–24,230 cal BP) at 95.4 % certainty. Two bone dates were too old to be modelled with the phases (UCIAMS-266006 and UCIAMS-266007). For the UCIAMS specimens, specimen ID (abbreviated to the last five digits), mitochondrial haplotype (if available), and biomolecular sex is included. (B) Mammoths were sexed using DNA (triangles) and proteomics (♀, ♂). The samples analysed using both methods are indicated by an asterisk. Genetic sex was determined by estimating the X chromosome:autosome coverage ratio (X:A ratio). Samples were determined as ♀ if X:A = > 0.8 and ♂ if X:A < = 0.7. Coloured symbols below the specimen IDs indicate the specimen was confidently identified with proteomics; symbols in grey indicate there was some uncertainty in proteomic sex assignment. A grey dot indicates specimens for which no amelogenin was identified and thus proteomic sexing was not possible. Based on the two approaches, we confidently identified a total of 17 ♀ and 13 ♂ among 30 mammoth individuals.

content ranged from 0.002 % to 26.5 %, with 23 samples having < 1 % endogenous content, nine samples 1–6 %, five samples with 6–9 %, and two samples with an endogenous content of 18.5 % and 26.5 % (Table S5).

3.3. Biomolecular sex assignments

For 23 of the 39 individuals that were DNA sequenced, which included seven of the radiocarbon dated specimens, we had enough DNA data to genetically determine sex (Table S3). We found 15 of the specimens were female and eight of the specimens were male (Fig. 3B). These samples all showed characteristic aDNA damage patterns (Fig. S3, S4),

except perhaps sample 18231, where the patterns were less clear. This was most likely as a result of the low number of reads that successfully mapped to chromosome 8 (n = 223) and the X chromosome (n = 311) (Table S5).

To increase the number of sex assignments, we applied a palaeoproteomic approach to the remaining samples. To check for consistency among the two biomolecular sexing methods, we used six specimens (three females and three males) already confidently sexed using DNA as a baseline reference, and analysed them again with the proteomic approach (Table S7). We found 100 % consistency between methods for the five samples for which sufficient data were available for proteomic sex assignment (Fig. 3B).

Five of the total of 21 specimens analysed using palaeoproteomics contained no AMELX or AMELY making proteomic sex assignment impossible; this included one of specimens already identified by DNA as male (Fig. 3B, Table S7). The proteomes suggest that no to very little dental enamel was provided, also given the absence of other enamel-specific proteins in each of these five extracts, and that they were instead composed of dentine and/or cementum, which generally do not contain amelogenin.

In contrast, the remaining 16 extracts contained peptide matches to collagen type I (COL1A1 and COL1A2), amelogenins (AMELX and AMELY), ameloblastin (AMBN), enamelin (ENAM), collagen type 17, alpha-1 (COL17A1), matrix metalloproteinase-20 (MMP20), albumin (ALB), odontogenic ameloblast-associated protein (ODAM), and/or amelotin (AMTN), indicating the recovery of an otherwise normal Pleistocene dental enamel proteome (Cappellini, 2019; Welker, 2020).

Based on the six reference specimens, we determined that a cut-off of a minimum of two unique peptides matching to AMELY and a minimum of 15 unique peptides matching to AMELX was required to confidently assign sex.

We confidently determined five males and two females of the 11 unknown specimens. We identified an additional two possible males (with one AMELY-specific peptide identified) and two possible females (with <15 AMELX-only peptides identified) (Fig. 3B, Table S7).

All confidently identified male individuals contained at least two unique peptides overlapping amelogenin position 46 (in relation to XP_049728859.1 for AMELX and XP_049729447.1 for AMELY), where AMELX contains an isoleucine (I) while AMELY contains an methionine (M). In addition, specimens 18238, 18224, and 18259 contained unique AMELY peptides matching to other amelogenin positions (P123L; I124V; Q138H; position in reference to AMELX followed by the homologous amino acid present in AMELY, for the accession numbers listed above).

Altogether, the biomolecular sexing resulted in the confident identification of 17 (57 %) females and 13 males (43 %) among 30 individuals (Fig. 3B, Tables S3, S7).

3.4. Mitochondrial genomes

We generated mitogenomes for 16 mammoth individuals, with coverage of 2.8x-715x (full sequencing statistics in Table S5). All samples all showed characteristic aDNA damage patterns (Fig. S3, S4).

For three samples, mitogenomes were compiled based on the shotgun sequencing data, with > 1000 DNA sequencing reads mapping to the mitogenome reference (18222, genetically identified as female; 18250, genetically identified as male; 18256, genetically identified as female). For 14 individuals, we assembled mitogenomes with the capture approach, with > 900 DNA sequencing reads for each sample mapping to the mitogenome reference (Tables S3, S5).

Specimen 18256 produced a mitogenome in both the shotgun and capture approaches, which were identical at all non-ambiguous bases. We retained the captured version of the mitogenome for this sample, as it had higher coverage (715x *vs* 3.9x) and contained fewer ambiguous bases.

Of the 16 mitogenomes, three had > 20 % N bases and were initially excluded from the haplotype analysis. The remaining 13 sequences were analysed with 147 publicly available mitogenomes representing all known woolly mammoth clades (Table S6). The combined data set of 160 mitogenomes represented 90 unique DNA sequences, termed haplotypes.

Based on the alignment with no control region, we identified six haplotypes among the 13 Kostenki-Ia mitogenomes: Hap13, 41, 42, 43, 74, and 89 (Fig. 4, Tables S3). Hap13 was the most common and found in five of the 13 individuals. It was also shared with the one available mitogenome from Kostenki (SP2401/KX176789.1; unknown Kostenki site number), which was molecularly dated to 32,572 yr old in the original publication (Chang et al., 2017), and which based on our molecular dating analysis was estimated at 26,969 yr old (95 % probability: 52,548 - 4561 yr old). Hap13 was also shared with three non-Kostenki mammoths – from the Kraków Spadzista site in Poland, which are dated to ~27,000 cal BP (Fellows Yates et al., 2017).

The three specimens with > 20 % N bases (18225, 18236, 18255) were analysed separately to determine their haplotype affiliation. As these mitogenomes had a large amount of missing data, their inclusion in the initial analysis would have greatly reduced the number of informative sites in the alignment, reducing the power of the haplotype analysis. The separate analysis of these mitogenomes indicated that all three had Hap13.

The other five haplotypes present in our samples were all unique to Kostenki-Ia (Fig. 4). Haplotypes 41, 42, and 74 were each shared by two Kostenki-Ia mammoths (although see comment on one variant in the d-loop of Hap42 below), and haplotypes 43 and 89 were each observed in only one individual (Fig. 4B).

The control region sequence was initially omitted from the mitogenome analysis due to misalignments and missing data. However, the region has a relatively fast mutation rate and is therefore more variable, and thus we analysed the d-loop specifically for the individuals sharing a haplotype (Hap13, 41, 42, 74), to investigate whether there were any single nucleotide polymorphisms (SNP) at this locus that might indicate different haplotypes.

For both Hap13 and 41, we found no SNPs in the control region, indicating the sequences across individuals were indeed identical. This included the three Kostenki specimens that had > 20 % N. For Hap13, also the published Kostenki individual (Chang et al., 2017) shared the control region sequence, as did two of the three Polish individuals; only sequence MF579947.1 from Kraków Spadzista differed with a T in its position 16,209, where the others have a C (or N).

The analysis of Hap42 revealed one variable site between individuals, with a C to T transition in specimen 18243 at position 15,609, supported by 109 sequencing reads with T, often in the middle of the reads, and one read with A; in specimen 18222, the C at position 15,609 was supported by its position in the middle of 3/3 reads. The high coverage at the site in specimen 18243, and the presence of the variable site in the middle of the reads, suggested this was a real SNP and not the result of ancient DNA damage. And thus our findings indicate that the two individuals with Hap42 do differ at one site, and in reality represent two distinct haplotypes.

Hap74 had two SNPs, with G to A and T to C transitions in specimen 18232 at position 16,294–16,295 relative to specimen 18251 (determined by 13x read coverage at that position). In specimen 18232, only three reads cover these positions, with one having GT and two having AC, but at the first two positions of the reads. Thus, the SNPs are likely due to ancient DNA damage, and we therefore infer that the samples in reality have the same haplotype.

Five of the six identified Kostenki haplotypes fall within woolly mammoth mitochondrial Clade 1/DE (Hap13, 41, 42, 43, 89; 11/13 individuals) (Fig. 4). The remaining haplotype falls within Clade 3/B2 (Hap74; 2/13 individuals).

3.5. Mitogenomes with radiocarbon dates

Five individuals had both a radiocarbon date and a mitogenome

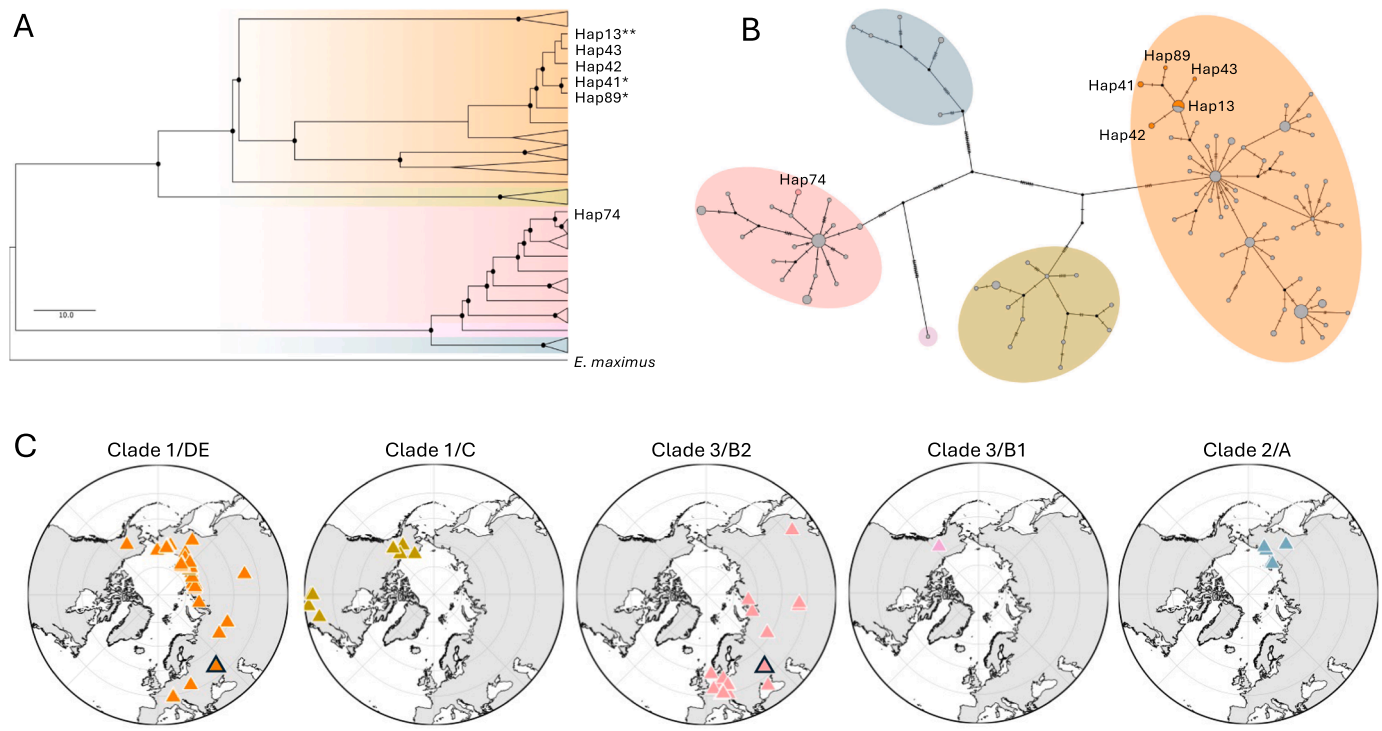

Fig. 4. Placement of the Kostenki mitogenome haplotypes within the global diversity of woolly mammoths. (A) Maximum likelihood phylogeny generated in IQ-TREE, with branch lengths transformed to proportional in Figtree. The alignment of 90 available woolly mammoth haplotypes, and the Asian elephant (*Elephas maximus*) as outgroup, contained 15,426 sites, of which 504 were parsimony informative. This analysis included the six Kostenki haplotypes present in the data when the control region was excluded; based on one SNP in the control region, Hap42 represents two haplotypes. The four reliable radiocarbon dates associated with individual haplotypes are indicated with an asterisk. Triangles represent collapsed branches. Black circles represent bootstrap support values > 70 %. (B) Median-joining haplotype network based on the alignment of the 13 Kostenki-Ia sequences (coloured) and the 147 available woolly mammoth mitogenomes (grey). The alignment contained 15,425 sites, of which 226 were variable. Sites with gaps or missing data were not considered. Each haplotype is indicated by a circle. The relative size of the circles represents the number of sequences of each haplotype. Black dots represent haplotypes not present in the data. Lines between haplotypes, which represent the evolutionary distance between two unique sequences, are not drawn to scale. The hatches on these lines show the number of substitutions between the haplotypes. (C) Maps showing the localities (coloured triangles) of the five mammoth clades shown in panels (A) and (B). The locality of Kostenki 11 is indicated by a black outline triangle in the maps of Clades 1/DE and 3/B2. Coordinates of the other localities were obtained from (Rambaut et al., 2018) or from the original publications (see Table S6). Four samples had unknown locations and are not included on the map. The map was produced using (Vihtakari, 2024).

(Table S3). However, the very young radiocarbon date of specimen 18222 was deemed unreliable, leaving four individuals with a radiocarbon date and a mitogenome.

The four individuals grouped in different phases (Fig. 3A):

Specimens 18239 (UCIAMS-266003; genetically identified as a female) and 18244 (UCIAMS-266004; genetically identified as a male) shared Hap13, but did not group in the same phase; 18244 grouped in Phase 1 and 18239 in Phase 2. Thus, our analysis indicated they are unlikely to be contemporaneous.

Specimen 18250 (UCIAMS-251307, genetically identified as a male) was the only Kostenki individual with Hap89, a novel haplotype unique to our data (Fig. 4B), and grouped in Phase 2.

Specimen 18256 (UCIAMS-266006; genetically identified as a female) had Hap41, another novel haplotype unique to our dataset (Fig. 4B). It was located at the outer rim of the complex (Fig. S2A) and was one of the two oldest samples identified at the site, and thus grouped apart from the two main phases of activity inferred from our Oxcal analysis.

Specimen 18233 also had Hap41. The specimen was located in the centre of the mammoth bone complex (Fig. S5), and our proteomic sexing identified it as a possible male (Fig. 3B, Table S7). We did not have a radiocarbon date for the specimen, but did estimate a molecular date (median: 23,396 years ago). However, the estimate had such a wide 95 % HPD interval (32,770–10,224 yr old), that we could not place the individual in a meaningful temporal context (Table S9).

3.6. Molecular dating

The molecular dating analyses converged for all ten samples, with ESS values > 200 for all parameters. All molecular dates are shown in Table S9, and the molecular dates of the Clade 1/2B mitogenomes are shown in Fig. S6 alongside the eight radiocarbon dates new to this study for comparison.

We observed wide probability distributions for all the molecular date estimates (Fig. S6, Table S9). The probability ranges always spanned an order of magnitude and were far wider than the probability ranges of the reliable radiocarbon dates from Kostenki 11-Ia (Tables S3, S4) and the inferred timespan of activity (Fig. 3A).

Only one median calendar age estimate fell within the 95.4 % certainty of the Kostenki 11-Ia specimens used in the Oxcal analysis: specimen 18228 = 24,031 yr old (Table S9). However, the wide 95 % probability (35,435 - 9059 yr old) meant it was not informative (Fig. S6).

The two Kostenki sequences from Clade 3/B2 had exceptionally old molecular dates: 18232 = 284,600 yr old (95 % probability: 519,870–85,355 yr old) and 18251 = 309,260 yr old (95 % probability: 544,250–86,889 yr old). This was not due to missing data in the mitogenomes (Table S9), but was most likely due to the fact that there was only one other mitogenome (KX027526) from this clade with a curated radiocarbon date from (Dehasque et al., 2021), which was subsequently excluded from the dating analysis as its median calibrated date was 50,000–40,000 cal BP. Consequently, 18232 and 18251 were the only representative of Clade 3/B2 in their respective dating analysis, possibly

leading to inaccurate date estimates due to a lack of context from other sequences of that clade.

Including all 13 sequences with calibrated radiocarbon dates between 50,000 and 40,000 cal BP resulted in younger estimates for these two mitogenomes, although still markedly older than the other Kostenki mitogenomes: 18232 = 50,186 yr old (95 % probability: 103,180–3049 yr old) and 18251 = 64,300 yr old (95 % probability: 119,410–7796 yr old). However, with these analyses, the root age estimate was substantially younger at around 3.88 million years ago (Ma) (95 % probability: 4.64–3.18 Ma), than the expected root age of 4.5–5.3 Ma (van der Valk et al., 2021).

Thus, the molecular dates for the mitogenomes were too imprecise to be informative for our purposes, and were not considered further.

3.7. Stable isotope analysis

We generated 38 δ^{13}C and δ^{15}N measurements from bone (n = 1) and dentine (n = 37) collagen of the Kostenki woolly mammoths (Fig. 5); sample 18253 did not yield enough collagen for stable isotope analysis. We combined our data from the 38 individuals with publicly available records from the species. Based on the overlap on the 95 % confidence ellipses and the average estimates, we did not observe any significant differences in isotopic composition between sexes within the Kostenki 11-Ia woolly mammoths (Fig. 5 A).

The published dataset comprised 378 woolly mammoths from E Beringia (n = 129), N Siberia (n = 183), Russian Plain (n = 16), and W/C Europe (n = 50), with sample ages from > 55,500 BP to 13,871 cal years BP (Table S8). The average δ^{13}C and δ^{15}N of the Kostenki mammoths falls close to values recorded for the Russian Plain and W/C Europe (Fig. 5B). When focusing only on samples from the LGM, the average isotopic composition of the Kostenki 11-Ia woolly mammoths are also closer to Russian Plain and W/C Europe woolly mammoths (Fig. 5 C).

4. Discussion

We performed biomolecular analysis of 39 woolly mammoth specimens sampled from the third mammoth bone structure at Kostenki 11-Ia. We radiocarbon dated nine specimens (one specimen was dated twice, totalling ten dates), and used the ages to interpret the time frame of human activity at the site. Combining genetic and proteomic methods, we sexed 30 individuals, and further contextualised the Kostenki 11-Ia specimens within the frameworks of available mitochondrial DNA and paleoecological (δ^{13}C and δ^{15}N) woolly mammoth data.

4.1. Dating human activity at the site

The 11 high-precision radiocarbon dates – which included mammoth teeth and charcoal – indicated the presence of three radiocarbon date groups, and in addition indicate two phases of human activity at the site (Fig. 3A). The dates new to this study indicate the newly-discovered presence of some older mammoth material at the site, in the form of two molars that are placed in the outer ring of the structure (Fig. S2).

Based on a smaller set of dates for Kostenki 11-Ia, Pryor et al (Pryor et al., 2020). reported evidence for two distinct clusters of dates at the third structure, and suggested this indicated either a single occupation phase plus a group of younger contaminated dates; or that there were two discrete occupation phases at the site. The expanded dataset presented here shows a similar pattern, whereby the high-precision radiocarbon dates can be divided into two distinct groups – Phase 1 aged 25,040–24,670 cal BP (95.4 % certainty) and Phase 2 aged 24,580–24,230 cal BP (95.4 % certainty; Fig. 3A).

The apparent hiatus between the two newly-defined phases is substantially less than that reported in Pryor et al (Pryor et al., 2020)., although it remains in the order of hundreds of years. It is notable that both identified phases are represented by dates on two different materials, and include mammoth specimens and charcoal recovered from various places within the third mammoth bone complex, potentially indicating human activity in both phases. A single additional radiocarbon date measured on burned bone gives further evidence of human activity within the same time window, but unfortunately lacked the precision required to associate this securely with either phase (NSKA-886; Supplementary Text). We further note that the oldest and only reliable available date for the first Kostenki 11-Ia complex (GIN-2532; 24,900–23,100 cal BP, 95.4 % certainty) correlates broadly with the Phase 2 dates of the third complex (Fig. S1), suggesting Phase 2 may have included activity at both the first and third Kostenki 11-Ia complexes, a point which warrants further investigation in future.

The discreteness of the radiocarbon dates into two phases is consistent with the discovery in 2014–2015 of a stratified area of burning at

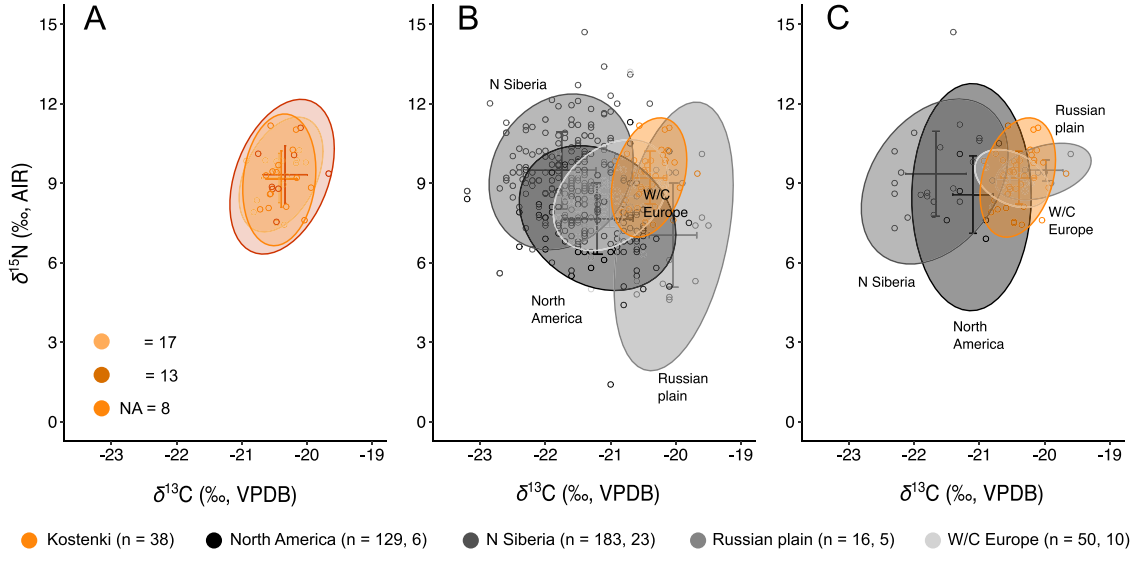

Fig. 5. δ^{13}C and δ^{15}N isotopic composition of woolly mammoths. Bivariate plot of the 38 Kostenki 11-Ia woolly mammoth isotopic compositions (A) by biomolecular sex; and in the context of (B) 378 published woolly mammoth isotopic records with ages from > 55,500 BP (infinite) to 13,871 cal BP (median age); and (C) woolly mammoth records from the Last Glacial Maximum only (28,660–20,520 cal BP). Sample sizes for each region are presented for both datasets, with (n = B, C). For (A), N/A indicates sex could not be determined. Ellipses represent 0.95 confidence levels. Crosses represent mean value ± s.d.

the site, which indicates two phases of activity (Dudin and Fedyunin, 2019). Our biomolecular data do not shed further light on this; of the individuals with both radiocarbon dates and mitogenomes, two shared a haplotype (Hap13), and had overlapping 95.4 % certainties, which could lend support to them being part of the same family group or matriline. However, the dates were grouped in different phases. Furthermore, Hap13 was the most prevalent haplotype – it was found in eight of our individuals, in addition to the available Kostenki mitogenome (Chang et al., 2017), and three Kraków Spadzista mammoths from Poland (Fellows Yates, 2017). However, our molecular dating resulted in very wide 95 % probabilities, rendering the dates uninformative for our purposes (Fig. S6). Although molecular dating can serve as an age proxy, our findings highlight a case where the lack of precision of the approach renders it inadequate to place individuals within the very narrow age range of the available radiocarbon dates from Kostenki-Ia (Fig. 3A).

Combined, our findings indicate two interpretations of the Phase 1/Phase 2 radiocarbon dates at Kostenki 11-Ia are possible, with the evidence indicating: (i) a single phase of human activity, that involved the use of already-old mammoth bones and wood hundreds of years old at the time humans brought them to the site, and/or the incomplete removal of contamination from some of the retained radiocarbon dates; or (ii) that there genuinely were two discrete phases of activity at Kostenki 11-Ia, separated by hundreds of years. Distinguishing these possibilities will require further investigation of the site's archaeology, especially an understanding of the stratigraphic context and material remains found there, to discern whether or not different phases of activity can be identified.

4.2. Modes of bone accumulation at Kostenki 11-Ia

Our biomolecular sexing showed a predominance of females among the mammoth specimens at Kostenki 11-Ia (♀ = 57 %, ♂ = 43 %; Fig. 3B, Table S3). Genetic sexing of mammoth bones collected across a large geographic area in NE Siberia identified a majority of males (n = 98; ♀ = 31 %, ♂ = 69 %) (Pečnerová et al., 2017a). This was explained by putative differences in behaviour of females and males, and the social structure of woolly mammoths (e.g., Maschenko et al., 2006); less experienced solitary males may have been more likely to be caught and die in natural traps, which favour preservation, and thus are overrepresented in the fossil record (Pečnerová et al., 2017a). The overrepresentation of females at Kostenki suggest the individuals were derived primarily from mammoth herds, which is supported by the presence of all age classes at the site; depending on area, the percentage of juveniles varies across the complex, from 3 % to 4 % to 10–15 % of the bones (Dudin, 2016; Dudin, 2017). If specimens were from natural traps only, we would expect more age uniformity, with mostly subadult and adult males.

Our radiocarbon evidence indicated the Kostenki 11-Ia mammoths died across several centuries. Thus, they did not represent a single-family group, which was further verified by our identification of seven mitochondrial haplotypes among 16 individuals (Fig. 4, Table S3). Several haplotypes were present in multiple individuals; Hap13 was found in eight Kostenki individuals, but our analysis showed the haplotype had a wider geographic range being also found in three Kraków Spadzista individuals from Poland, and thus was not informative for informing on familial relationships.

Hap41 was unique to our dataset and present in two individuals, which could suggest the individuals were related, as the mitochondrial genome is passed from mother to offspring. However, only one of the samples (18256; UCIAMS-266006; female) was radiocarbon dated. The molecular age of the other sample (18233; median age 23,371 years ago) had such a wide 95 % probability interval that it was not informative for reliably placing the individual in a temporal context (Fig. S6, Table S9). Thus, based on the available data we could not evidence if the mammoths sharing Hap41 are from the same family group or matriline, which would be supported by similar ages.

Only a small number of the bones excavated in the structure are articulated, primarily vertebral bones (Dudin and Fedyunin, 2019), suggesting the mammoths did not die on site. This pattern differs from the woolly mammoths at the Sevsk family group site (Bryansk Region, Russia), which were partially or completely articulated (Maschenko et al., 2006). Thus, we suggest the woolly mammoths at Kostenki 11-Ia died off-site, and were harvested and moved to the structure. Indeed, the lower fraction of juveniles present at Kostenki 11-Ia relative to bone beds of a herd or a whole population – where the number of juveniles comprise ~40 % of the individuals (Haynes, 2017) – may suggest the preferential acquisition of adult individuals.

Our analysis identified two new dates measured on mammoth specimens from the third structure that were much older than the rest; UCIAMS266007 (18257; genetically sexed as a male) and UCIAMS266006 (18256; genetically sexed as a female), aged 25,662–24,802 and 25,798–25,140 cal BP (95.4 % certainty), respectively (Fig. 3A; Table S3). The mandibles were positioned along the outer edge of the ring of bones making up the eastern wall of the structure (Fig. S2). The ages were too old to be modelled with Phase 1 dates, being 0–1300 years older, and 200–1500 years older than Phase 2 dates (95.4 % certainty, Fig. 3A). Interestingly, the youngest of these two older samples 18256) shared Hap41 with another individual (18233) at the site, which was placed in the centre of the structure (Fig. S5). Specimen 18233 was not dated, and the estimated molecular age had too wide probability intervals to be informative, and thus we could not place it in a relevant temporal context (Fig. S6, Table S9).

We are confident the two older dates do not conform with the main phases of human occupation at the site, due to the strength of evidence constraining the two inferred phases (i.e., number of individual dates) and, in addition, the extended period of human activity suggested by their inclusion is not supported by the archeology of the site (Pryor et al., 2020). We are also confident that the two older mandibles were not redeposited from older sedimentary layers at Kostenki 11-Ia due to their position within the ring of bones defining the structure (Fig. S2). Redeposition has been reported in the mammoth bone assemblage of Achchagyi–Allaikha (Yana-Indighirka coastal lowlands, Siberia), where a specimen ~24,000 yr older than any other mammoth radiocarbon dates at the site was interpreted as a redeposition from an older sedimentary layer (Nikolskiy et al., 2010). However, the evident stratigraphic integrity of Kostenki 11-Ia argues against this.

Rather, we interpret our dates as evidence that the two oldest-dated mandibles were scavenged from long-dead carcasses of mammoth, and brought to Kostenki 11–1a as 'fossil' raw bone material by the humans that built the structure. The older material may have been scavenged from other Kostenki sites, where both natural and human-created mammoth bone beds have been discovered (e.g., in Kostenki 5-layer II, a natural bone bed with dates from ~28,000–24,500 cal BP; reviewed in Petrova et al., 2023).

Based on the available data, we are unable to elucidate if the Kostenki 11-Ia mammoths were also derived from active human hunting. Human exploitation of mammoth bones and ivory from natural accumulations has been documented elsewhere on the basis of radiocarbon dating evidence (e.g., Pitulko et al., 2014), and has been widely discussed at a theoretical level in the context of the circular mammoth bone features (e.g., Soffer, 2003; Svoboda et al., 2005). However, to our knowledge, our analysis provides what may be the first direct evidence indicating the use of scavenged skeletal material in the construction of a circular mammoth bone feature, and is thus a significant finding that adds to our understanding of how these sites were created.

4.3. Phylogeography and palaeoecology of the Kostenki 11-Ia mammoths

The 16 mitochondrial genomes retrieved from our specimens represented six haplotypes when the alignment excluded the d-loop, and seven haplotypes when the d-loop was included. We only considered the

six haplotypes (and no d-loop) in our phylogeographic analysis (Fig. 4A, B). The global phylogeography of mammoth mitochondrial genomes indicates three main clades, which are further subdivided into several subclades that are somewhat geographically distinct (e.g., Chang, 2017; Debruyne, 2008; Fellows Yates, 2017; Wang, 2021). Our sequences grouped in Clade 1/DE and Clade 3/B2, in agreement with their known geographic distribution (Fig. 4C).

Our analysis indicated that five haplotypes were distinct to Kostenki 11-Ia, four of which grouped within Clade 1/DE, which has been reported in mammoths across Eurasia and Alaska (Table S6, Chang, 2017; Fellows Yates, 2017). One Kostenki haplotype (found in two of our specimens) grouped in Clade 3/B2, which has been reported in mammoths across Eurasia, with median ages between 48,125 and 24,511 cal BP. However, only one Clade 3/B2 sequence (KX027526) had a radiocarbon date curated by (Dehasque et al., 2021), with an age of 45, 294 cal BP (Table S6). The samples with the youngest radiocarbon dates of this clade are from present-day Germany, and range from 38,336 to 24,511 cal BP (Table S6, Chang, 2017; Fellows Yates, 2017). Assuming the two Kostenki 11-Ia individuals in Clade 3/B2 are the same age as the other mammoths at this site (25,465–24,390 cal BP), and not the age estimated with molecular dating (~300,000 yr old), they represent some of the youngest members of this clade in western Europe, indicating its survival into the LGM in this region.

Foraging differences between sexes have been reported for African elephants, based on behavioural observations and measurements of feeding impact on the tree canopy, and are influenced by body size, reproductive strategies, and social structure (Shannon et al., 2006). Foraging differences between females and males have also been described for Asian elephants (Sukumar and Gadgil, 1988). Based on bone and dentine collagen $\delta^{13}C$ and $\delta^{15}N$, we did not detect differences in stable isotope composition between sexes (Fig. 5 A). This finding suggests a lack of resource partitioning between females and males in woolly mammoths and provides, to our knowledge, the first attempt to investigate differences in foraging ecology between sexes in mammoths, and indeed in any Late Pleistocene megafaunal remains.

The coarse nature of our data is such that fine-scale differences cannot be identified. Bone and dentine collagen $\delta^{13}C$ and $\delta^{15}N$ provides insights into long-term foraging averaged over years to decades, but does not provide information on what species comprise the diet (e.g., Bocherens, 2003). Furthermore, median calibrated ages of the radiocarbon dates of our samples span 1800 years, from 23,995 to 25,798 cal BP (95.4 % certainty; Table S3), which may mask temporal differences and not fully capture mammoth foraging strategies.

However, when comparing $\delta^{13}C$ and $\delta^{15}N$ among species, they can be used to identify differences in foraging or how environmental factors differentially affect species foraging ecology. For instance, based on $\delta^{15}N$, mammoths have a distinct isotopic composition compared to other herbivores (e.g., horse), which may reflect different plant type or plant part preferences (Schwartz-Narbonne et al., 2019). Mammoths are known to show regional differences in $\delta^{13}C$ and $\delta^{15}N$ isotopic composition (e.g., Arppe et al., 2019). When we consider only mammoths from the LGM, the Kostenki 11-Ia data show similar average values to mammoths from the Russian plain (Eurasia lower latitudes $<60°N$) and W/C Europe (Fig. 5 C). Thus, the isotopic composition of the Kostenki mammoths agrees with their geographic location.

5. Conclusions

Our study provides new insight into the archeological context of the mammoth bone structures of the central European Plain, and the Palaeolithic humans associated with them. The eight new reliable radiocarbon dates presented in this study confirmed the third structure at Kostenki 11-Ia is among the oldest circular mammoth bone structures yet discovered. Furthermore, the dates indicate that human activity at the site may have spanned several centuries, potentially occurring in two discrete phases. Alternatively, it may have involved the collection of already-ancient bones and wood from across the landscape. In combination with the archaeology of the site, our data suggest the mammoth bones were acquired off-site, and included at least some degree of scavenging from bone beds and of opportunistic finds of long-dead individuals. Our findings also provide novel insights on the absence of isotopically-differentiated resource use by female and male woolly mammoths, providing to our knowledge the first analysis of foraging differences between sexes in any Late Pleistocene megafauna.

CRediT authorship contribution statement

Matthew Teeter: Writing – review & editing, Investigation. **Ashot Margaryan:** Writing – review & editing, Investigation. **Ruslan Khaskhanov:** Writing – review & editing, Investigation. **Louise Le Meillour:** Writing – review & editing, Investigation. **Deon de Jager:** Writing – review & editing, Visualization, Investigation. **Gaudry Troché:** Writing – review & editing, Investigation. **Alba Rey-Iglesia:** Writing – original draft, Visualization, Methodology, Investigation, Formal analysis, Conceptualization. **Frido Welker:** Writing – original draft, Formal analysis. **Paul Szpak:** Writing – original draft, Investigation, Formal analysis. **Eline Lorenzen:** Writing – original draft, Visualization, Supervision, Resources, Methodology, Investigation, Funding acquisition, Conceptualization. **Alexander Dudin:** Writing – review & editing, Investigation. **Alexander Pryor:** Writing – original draft, Visualization, Methodology, Investigation, Formal analysis, Conceptualization. **Tess Wilson:** Writing – review & editing, Investigation.

Declaration of Competing Interest

The authors declare that they have no known competing financial interests or personal relationships that could have appeared to influence the work reported in this paper.

Acknowledgements

We thank Eske Willerslev for his help in facilitating the field sampling campaign to Kostenki-11 by EDL and AM in August 2015, and Michelle Christel Larsen for her contribution to DNA data generation. We also thank Natasha Reynolds for helpful discussions regarding modelling of activity phases in Oxcal, and Wenxi Li for helpful input to the molecular dating analysis. **Funding:** This work was funded by the Villum Foundation Young Investigator Programme grant no. 13151 and grant no. 35372 to EDL and an NSERC Discovery Grant (2020–04740) to PS. FW is supported through funding from the European Research Council (ERC) under the European Union's Horizon 2020 research and innovation programme, grant agreement no. 948365. LLM is supported by a Marie Skłodowska-Curie postdoctoral fellowship funded by the European Union's Horizon 2020 research and innovation programme (grant agreement No 101062449).

Appendix A. Supporting information

Supplementary data associated with this article can be found in the online version at doi:10.1016/j.qeh.2024.100049.

References

Allentoft, M.E., et al., 2015. Population genomics of Bronze Age Eurasia. Nature 522, 167–172.
Arppe, L., et al., 2019. Thriving or surviving? The isotopic record of the Wrangel Island woolly mammoth population. Quat. Sci. Reviews 222, 105884.
Bache, N., et al., 2018. A novel LC system embeds analytes in pre-formed gradients for rapid, ultra-robust proteomics. Mol. Cell. Proteom. 17, 2284–2296.
Balasse, M., Tresset, A., 2002. Early weaning of Neolithic domestic cattle (Bercy, France) revealed by intra-tooth variation in nitrogen isotope ratios. J. Archaeol. Sci. 29, 853–859.
Beaumont, W., Beverly, R., Southon, J., Taylor, R.E., 2010. Bone preparation at the KCCAMS laboratory. Nucl. Instrum. Methods Phys. Res. B 268, 906–909.

Bocherens, H., 2003. Isotopic biogeochemistry and the palaeoecology of the mammoth steppe fauna. Deinsea 9, 57–76.
Bonafini, M., Pellegrini, M., Ditchfield, P., Pollard, A.M., 2013. Investigation of the "canopy effect" in the isotope ecology of temperate woodlands. J. Archaeol. Sci. 40, 3926–3935.
Bro-Jørgensen, M.H., et al., 2021. Genomic sex identification of ancient pinnipeds using the dog genome. J. Archaeol. Sci. 127, 105321.
Bronk Ramsey, C., OxCal v. 4.4. 4 [software]. URL: https://c14. arch. ox. ac. uk/oxcal. html (2021).
Cappellini, E., et al., 2019. Early Pleistocene enamel proteome from Dmanisi resolves Stephanorhinus phylogeny. Nature 574, 103–107.
Chang, D., et al., 2017. The evolutionary and phylogeographic history of woolly mammoths: a comprehensive mitogenomic analysis. Sci. Rep. 7.
Cintas-Peña, M., et al., 2023. Amelogenin peptide analyses reveal female leadership in Copper Age Iberia (c. 2900–2650 BC). Sci. Rep. 13, 9594.
Crann, C.A., Murseli, S., St-Jean, G., Zhao, X., Clark, I.D., Kieser, W.E., 2017. First status report on radiocarbon sample preparation techniques at the AE Lalonde AMS Laboratory (Ottawa, Canada). Radiocarbon 59, 695–704.
Dabney, J., et al., 2013. Complete mitochondrial genome sequence of a Middle Pleistocene cave bear reconstructed from ultrashort DNA fragments. Proc. Natl. Acad. Sci. U. S. A. 110, 15758–15763.
Debruyne, R., et al., 2008. Out of America: ancient DNA evidence for a new world origin of late quaternary woolly mammoths. Curr. Biol. 18, 1320–1326.
Dehasque, M., et al., 2021. Combining Bayesian age models and genetics to investigate population dynamics and extinction of the last mammoths in northern Siberia. *Quat. Sci. Rev.* 259, 106913.
Dinnis, R., et al., 2018. The Age of the 'Anosovka-Tel'manskaya Culture' and the Issue of a Late Streletskian at Kostënki 11. SW Russ. *PPS* 84, 21–40.
Dinnis, R., et al., 2019. New data for the early Upper Paleolithic of Kostenki (Russia). J. Hum. Evol. 127, 21–40.
Dudin, A.E., Fedyunin, I.V., 2019. "Kostenki 11 (Anosovka 2): the third bone-earthen complex of the cultural layer Ia. In: Platonova, N.I., Lisitsyn, S.N. (Eds.), in Man and mammoth in Palaeolithic Europe: in memory of Mikhail Vasilyevich. Branco, in Russian, pp. 221–236.
Dudin, A.E., Report on the excavations of the multilayer Paleolithic site Kostenki 11 (Anosovka 2) in the Khokholsky district of the Voronezh region in 2016 - F-1, R-1, No. 52172 (2016) (in Russian).
Dudin, A.E., Report on the excavations of the multilayer Paleolithic site Kostenki 11 (Anosovka 2) in the Khokholsky district of the Voronezh region in 2017 - F-1, R-1, No. 58042 (2017) (in Russian).
Enk, J., et al., 2016. Mammuthus population dynamics in late pleistocene north america: divergence, phylogeography, and introgression. Front. Ecol. Evol. 4, 42.
Fedyunin, I.V., O raskopkakh mnogosloynoy paleoliticheskoy stoyanki Kostonki 11 (Anosovka 2) v Khokhol'skom rayone Voronezhskoy oblasti v 2015 g. Voronezh: LLC'TERRA (2016) (in Russian).
Fellows Yates, J.A., et al., 2017. **Central european woolly mammoth population dynamics: Insights from late pleistocene mitochondrial genomes**. Sci. Rep. 7, 17714.
Gavrilov, K.N., 2015. Dwellings" of the anosovo-mezin type: origins and interpretation. Strat. J. 1.
Hartman, G., 2011. Are elevated δ^{15}N values in herbivores in hot and arid environments caused by diet or animal physiology? Func. Ecol. 25, 122–131.
Haynes, G., 2017. Finding meaning in mammoth age profiles. Quat. Int. 443, 65–78.
Herrando-Pérez, S., 2021. Bone need not remain an elephant in the room for radiocarbon dating. R. Soc. Open Sci. 8, 201351.
Hoang, D.T., Chernomor, O., Von Haeseler, A., Minh, B.Q., Vinh, L.S., 2018. UFBoot2: improving the ultrafast bootstrap approximation. Mol. Biol. Evol. 35, 518–522.
Iakovleva, L., 2015. The architecture of mammoth bone circular dwellings of the Upper Palaeolithic settlements in Central and Eastern Europe and their socio-symbolic meanings. Quat. Int. 359, 324–334.
Iakovleva, L., 2016. Mezinian landscape system (Late Upper Palaeolithic of Eastern Europe). Quat. Int. 412, 4–15.
Jónsson, H., Ginolhac, A., Schubert, M., Johnson, P.L.F., Orlando, L., 2013. mapDamage2.0: fast approximate Bayesian estimates of ancient DNA damage parameters. Bioinformatics 29, 1682–1684.
Kalyaanamoorthy, S., et al., 2017. ModelFinder: fast model selection for accurate phylogenetic estimates. Nat. Met. 14, 587–589.
Kapp, J.D., Green, R.E., Shapiro, B., 2021. A fast and efficient single-stranded genomic library preparation method optimized for ancient DNA. J. Hered. 112, 241–249.
Katoh, K., Standley, D., 2013. MAFFT multiple sequence alignment software version 7: improvements in performance and usability. Mol. Biol. Evol. 30, 772–780.
Kearse, M., et al., 2012. Geneious Basic: an integrated and extendable desktop software platform for the organization and analysis of sequence data. Bioinformatics 28, 1647–1649.
Kuitems, M., van Kolfschoten, T., Tikhonov, A.N., van der Plicht, J., 2019. Woolly mammoth δ^{13}C and δ^{15}N values remained amazingly stable throughout the last~ 50,000 years in north-eastern Siberia. Quat. Int. 500, 120–127.
Leigh, J.W., Bryant, D., 2015. popart: full-feature software for haplotype network construction. Methods Ecol. Evol. 6, 1110–1116.
Li, H., et al., 2009. The sequence alignment/map format and SAMtools. Bioinformatics 25, 2078–2079.
Li, H., Durbin, R., 2009. Fast and accurate short read alignment with Burrows-Wheeler transform. Bioinformatics 25, 1754–1760.
Lister, A.M., Agenbroad, L.D., 1994. Gender determination of the Hot Springs mammoths. In: Agenbroad, L.D., Mead, J.I. (Eds.), in *The Hot Springs Mammoth Site: a decade of field and laboratory research in paleontology, geology, and paleoecology*. Fenske Printing, pp. 208–214.
Maddison, W.P., Maddison, D.R., Mesquite: a modular system for evolutionary analysis. Version 3.81 (2023) ⟨http://www.mesquiteproject.org⟩.
Marquer, L., et al., 2012. Charcoal scarcity in Epigravettian settlements with mammoth bone dwellings: the taphonomic evidence from Mezhyrich (Ukraine). J. Archaeol. Sci. 39, 109–120.
Martinez De La Torre, H.A., Reyes, A.V., Zazula, G.D., Froese, D.G., Jensen, B.J., Southon, J.R., 2019. Permafrost-preserved wood and bone: Radiocarbon blanks from Yukon and Alaska. Nucl. Instrum. Methods Phys. Res. 455, 154–157.
Maschenko, E.N., Gablina, S.S., Tesakov, A.S., Simakova, A.N., 2006. The Sevsk woolly mammoth (*Mammuthus primigenius*) site in Russia: Taphonomic, biological and behavioral interpretations. Quat. Int. 142, 147–165.
Meyer, M., Kircher, M., 2010. Illumina sequencing library preparation for highly multiplexed target capture and sequencing. db.prot5448 Cold Spring Harb. Protoc. (6) db.prot5448.
Minh, B.Q., et al., 2020. IQ-TREE 2: new models and efficient methods for phylogenetic inference in the genomic era. Mol. Biol. Evol. 37, 1530–1534.
Murphy, B.P., Bowman, D.M.J., 2006. Kangaroo metabolism does not cause the relationship between bone collagen δ^{15}N and water availability. Func. Ecol. 20, 1062–1069.
Nikolskiy, P.A., Basilyan, A.E., Sulerzhitsky, L.D., Pitulko, V.V., 2010. Prelude to the extinction: Revision of the Achchagyi–Allaikha and Berelyokh mass accumulations of mammoth. Quat. Int. 219, 16–25.
Palkopoulou, E., et al., 2013. Holarctic genetic structure and range dynamics in the woolly mammoth. Proc. R. Soc. B 280, 20131910.
Parker, G.J., et al., 2019. Sex estimation using sexually dimorphic amelogenin protein fragments in human enamel. J. Archaeol. Sci. 101, 169–180.
Pečnerová, P., et al., 2017a. Genome-based sexing provides clues about behavior and social structure in the woolly mammoth. Curr. Biol. 27, 3505–3510.
Pečnerová, P., et al., 2017b. Mitogenome evolution in the last surviving woolly mammoth population reveals neutral and functional consequences of small population size. Evol. Lett. 1, 292–303.
Petrova, E.A., Voyta, L.L., Bessudnov, A.A., Sinitsyn, A.A., 2023. An integrative paleobiological study of woolly mammoths from the Upper Paleolithic site Kostenki 14 (European Russia). Quat. Sci. Rev. 302, 107948.
Pitulko, V.V., Basilyan, A.E., Pavlova, E.Y., 2014. The Berelekh Mammoth "Graveyard": new chronological and stratigraphical data from the 2009 field season. Geoarchaeology 29, 277–299.
Popov, V.V., et al., 2004. "Kostenki 11 (Anosovka 2). In: Anikovich, M.V., Platonova, N.I. (Eds.), in Kostenki & the early Upper Palaeolithic of Eurasia: general trends, local developments. Institute for the Material Culture History, in Russian, pp. 6–17.
Praslov, N.D., Soulerjytsky, L.D., 1997. De nouvelles données chronologiques pour le paléolithique de Kostienki-sur-Don. Pr. éHist. Eur. éenne 11, 133–143 (in French).
Pryor, A.J.E., et al., 2020. The chronology and function of a new circular mammoth-bone structure at Kostenki 11. Antiquity 94, 323–341.
Puzachenko, A.Y., et al., 2017. The Eurasian mammoth distribution during the second half of the Late Pleistocene and the Holocene: Regional aspects. Quat. Int. 445, 71–88.
RambautA., FigTree v1. 3.1. (2009) ⟨http://tree.bio.ed.ac.uk/software/figtree/⟩.
Rambaut, A., Drummond, A.J., Xie, D., Baele, G., Suchard, M.A., 2018. Posterior Summarization in Bayesian Phylogenetics Using Tracer 1.7. Syst. Biol. 67, 901–904.
Reimer, P.J., et al., 2020. The IntCal20 northern hemisphere radiocarbon age calibration curve (0–55 cal kBP). Radiocarbon 62, 725–757.
Reynolds, N., Dinnis, R., Bessudnov, A.A., Devièse, T., Higham, T., 2017. The Kostënki 18 child burial and the cultural and funerary landscape of Mid Upper Palaeolithic European Russia. Antiquity 91, 1435–1450.
Rogachev, A.N., Popov, V.V., 1982. in Russian). In: Praslov, N.D., Rogachev, A.N. (Eds.), Kostenki 11 (Anosovka 2). Nauka, pp. 116–132.
Rohland, N., Hofreiter, M., 2007. Ancient DNA extraction from bones and teeth. Nat. Protoc. 2, 1756–1762.
Rozas, J., et al., 2017. DnaSP 6: DNA sequence polymorphism analysis of large data sets. Mol. Biol. Evol. 34, 3299–3302.
Sablin, M., Reynolds, N., Iltsevich, K., Germonpré, K.M., 2023. The epigravettian site of yudinovo, russia: mammoth bone structures as ritualised middens. Environ. Archaeol. 1–21.
Schubert, M., et al., 2012. Improving ancient DNA read mapping against modern reference genomes. BMC Genom. 13, 1–15.
Schubert, M., et al., 2014. Characterization of ancient and modern genomes by SNP detection and phylogenomic and metagenomic analysis using PALEOMIX. Nat. Protoc. 9, 1056–1082.
Schubert, M., Lindgreen, S., Orlando, L., 2016. AdapterRemoval v2: rapid adapter trimming, identification, and read merging. BMC Res. Notes 9, 88.
Schwartz-Narbonne, R., et al., 2019. Reframing the mammoth steppe: insights from analysis of isotopic niches. Quat. Sci. Rev. 215, 1–21.
Shannon, G., Page, B.R., Duffy, K.J., Slotow, R., 2006. The role of foraging behaviour in the sexual segregation of the African elephant. Oecologia 150, 344–354.
Sinitsyn, A.A., 2015. Perspectives on the Palaeolithic of Eurasia: Kostenki and related sites. World Herit. Heads 4, 163.
Sinitsyn, A.A., Praslov, N.D., Svezhentsev, I.S., Sulerzhitskii, L.D., Радиоуглеродная хронология верхнего палеолита Восточной Европы [Radiocarbon chronology of the Palaeolithic of Eastern Europe]. Радиоуглеродная хронология палеолита Восточной Европы и Северной Азии. ПроблеМы и перспективы, 21-66 (1997) (in Russian).
Smith, B.N., Epstein, S., 1971. Two categories of ^{13}C/^{12}C ratios for higher plants. Plant Physiol. 47, 380–384.

Soffer, O., 2003. "Mammoth bone accumulations: Death sites? Kill sites? Dwellings? In: Vasil'ev, S.A., Soffer, O., Kozlowski, J. (Eds.), in Perceived landscapes and built environments: the cultural geography of Last Paleolithic Eurasia. Archaeopress, Oxford, pp. 39–46.

Stewart, N.A., Gerlach, R.F., Gowland, R.L., Gron, K.J., Montgomery, J., 2017. Sex determination of human remains from peptides in tooth enamel. Proc. Natl. Acad. Sci. U. S. A 114, 13649–13654.

Suchard, M.A., Lemey, P., Baele, G., Ayres, D.L., Drummond, A.J., Rambaut, A., 2018. **Bayesian phylogenetic and phylodynamic data integration using BEAST 1.10**. Virus Evol 4.

Sukumar, R., Gadgil, M., 1988. Male-female differences in foraging on crops by Asian elephants. Anim. Behav.

Svoboda, J., Péan, S., Wojtal, P., 2005. Mammoth bone deposits and subsistence practices during Mid-Upper Palaeolithic in Central Europe: three cases from Moravia and Poland. Quat. Int. 126, 209–221.

Swift, J., et al., 2019. Micro methods for megafauna: novel approaches to late quaternary extinctions and their contributions to faunal conservation in the anthropocene. Bioscience 69, 877–887.

van der Valk, T., et al., 2021. Million-year-old DNA sheds light on the genomic history of mammoths. Nature 591, 265–269.

Vihtakari, M. ggOceanMaps: Plot Data on Oceanographic Maps using 'ggplot2'. Preprint at ⟨https://mikkovihtakari.github.io/ggOceanMaps/⟩ (2024).

Wang, Y., et al., 2021. Late Quaternary dynamics of Arctic biota from ancient environmental genomics. Nature 600, 86–92.

Welker, F., et al., 2020. The dental proteome of Homo antecessor. Nature 580, 235–238.

Wickham, H., 2011. ggplot2. Wiley Interdiscip. Rev. Comput. 3, 180–185.

Wittemyer, G., Getz, W.M., Vollrath, F., Douglas-Hamilton, I., 2007. Social dominance, seasonal movements, and spatial segregation in African elephants: a contribution to conservation behavior. Behav. Ecol. Sociobiol. 61, 1919–1931.